

Table 2. Material properties of the subsoil

Parameter	Name	Clay (CL)	Peat (OL)	Clay (CL)	Silt (ML)	Clay (CH)	Clay (CL)	Unit
Material model	Model	SSC	SSC	SSC	SSC	SSC	SSC	-
Type of material behaviour	Type	Undrained	Undrained	Undrained	Undrained	Undrained	Undrained	-
Soil unit weight above p.l.	γ_{sat}	15.5	14.8	15.5	13.4	12.6	11.1	kN/m ³
Soil unit weight below p.l.	γ_{sat}	17	18	16	18.6	17.7	15	kN/m ³
Horizontal permeability	k_x	3E-5	3.5E-4	1E-4	3.8E-4	6.65E-4	3.09E-4	m/day
Vertical permeability	k_y	3E-5	3.5E-4	1E-4	3.8E-4	6.65E-4	3.09E-4	m/day
Modified compression index	λ^*	0.06	0.12	0.07	0.075	0.064	0.098	-
Modified swelling index	k^*	0.015	0.037	0.02	0.02	0.015	0.019	-
Secondary compression index	μ^*	0.0025	0.003	0.0028	0.0031	0.0029	0.0033	-
Cohesion	c	10	5	10	3	12	14	kN/m ²
Friction angle	ϕ	22	30	20	22	14	24	degree
Over consolidation ratio	OCR	1	1.27	1	1	1	1.54	-

Table 3. Material properties of the columns

Parameter	Unit	Cement-column	Lime-column
Material model	-	Elastic	Elastic
Type of material behavior	-	Non-porous	Non-porous
Axial stiffness	kN/m	1.26E+04	2520.5
Flexural rigidity	kNm ² /m	132.35	26.47
Poisson's ratio	-	0.3	0.3

Numerical simulations by means of finite element method (FEM) have become a valuable tool in geotechnical engineering to predict and understand the behavior of complex structures. In the current study, by finite element (FE) code PLAXIS, the embankment material and subsoil were studied by 2D model under drained and undrained conditions, respectively. Modeling techniques in this 2D FE simulation

such as material type, element type, boundary conditions, and interface were similar to those used in the validation of physical investigation. To gain real and more empirical results, typical values of column dimensions and spacing in engineering practice were used. Medium mesh mode was used in the present work and, in more sensitive zones, mesh dimension got finer. The two-dimensional (2D) numerical model for this case study using Plaxis^{2D} software is shown in Fig. 2. It is note that the bottom and sides of the model were introduced by no-flow boundaries.

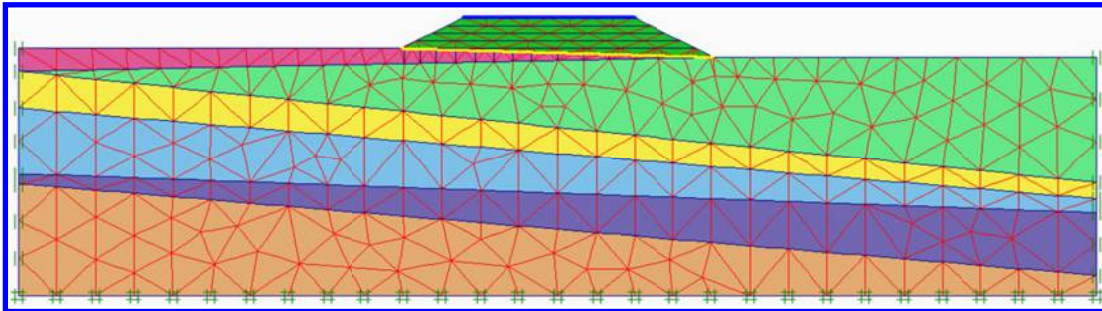


FIG. 2. The two-dimensional (2D) numerical model of the embankment

In the current study, the embankment fill and in-situ soils were modeled as linearly elastic-perfectly plastic materials with the Mohr–Coulomb failure criterion, while the columns were assumed to be linearly elastic materials. The Mohr–Coulomb model requires five parameters: effective cohesion, c' , friction angle, ϕ' , dilatancy angle, ψ , effective Young's modulus, E , and Poisson's ratio, ν . The parameters used in the analyses are summarized in Tables 1 through 3.

Results and discussion

The symbols used to abbreviate the analyzed systems were

NC: Non-column (untreated form)

CC: A combination of soil-cement columns

LC: A combination of soil-lime columns

CC-LC: A combination of soil-lime and soil-cement columns

As an overall conclusion, by comparing the settlement values of the embankment with and without columns, it can be stated that settlement values of the embankment significantly decreased when using columns, which represented the effective role of this system in improving the soft soil properties. However, differential settlement was observed between left and right sides of the embankment in some arrangements.

Fig. 3 is presented in order to compare the performance of all the systems (i.e., NC, CC, LC, and CC-LC). As shown in this figure, the systems with columns had a significant effect in reduction of total settlement. Also, maximum reduction in total settlement occurred with CC system and using CC-LC system caused maximum uniform settlement.

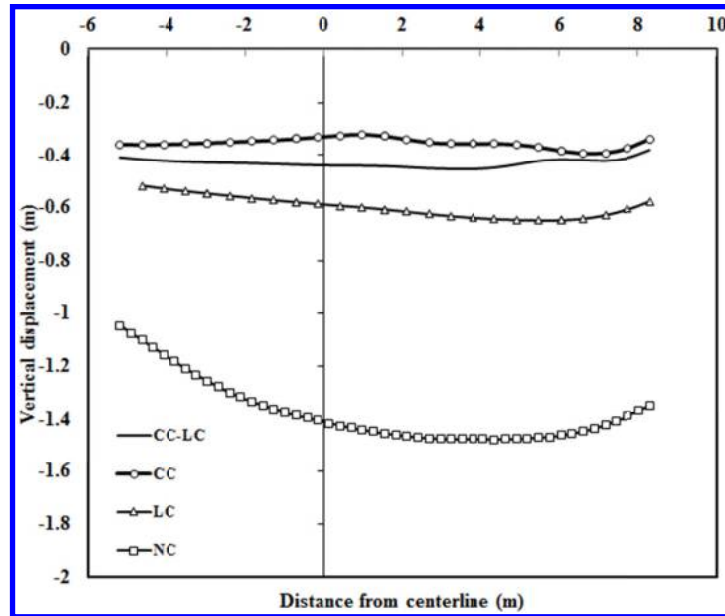


FIG. 3. The results of the combination of lime and cement columns model

In Fig. 4, settlement versus time is presented for all the system at three points (A, B, and C), where A, B, and C points are located on the left, central, and right sides of the embankment, respectively. As shown in Fig. 4, the improving systems had a more effect on the right side rather than left side or center of the embankment, which could be due to a thicker loose layer on the right side. As expected, the CC system had maximum impact on the settlement reduction of the embankment. Also, it can be seen that settlement was the largest for A, followed by B and then C.

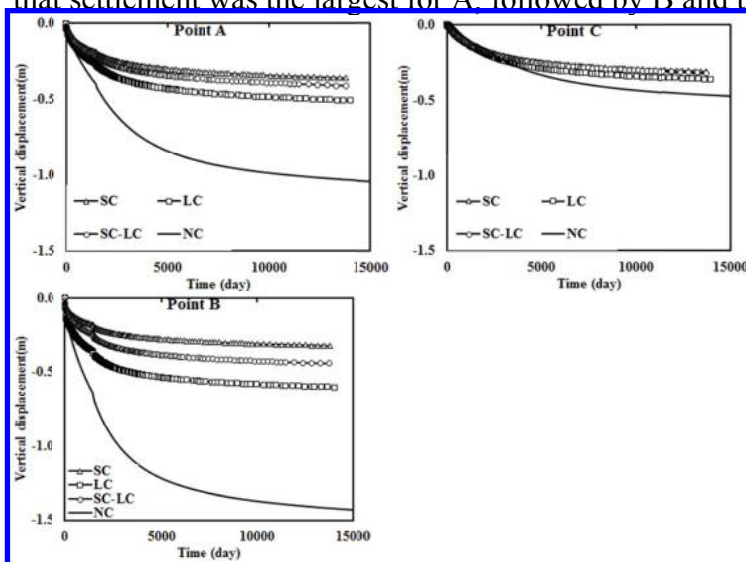


FIG. 4. Settlement of various points of the ground surface

Conclusion

In this study, two-dimensional finite element analyses were used to investigate the consolidation behavior of a road embankment constructed on a multi-column composite foundation with or without geosynthetic reinforcement.

Three systems, CC (soil-cement columns), LC (soil-lime columns), and CC-LC (a combination of soil-lime and soil-cement columns) were used to support the embankment fill and to mobilize the strength and stiffness of the soil at shallow depths.

Multi-column ground treatment can significantly reduce total and differential settlements of the embankment and increase embankment stability. Optimal arrangement of columns in CC, LC, and CC-LC systems was different so that CC and CC-LC systems with fewer columns had better performance than LC system.

CC and CC-LC systems are made the same settlement reduction, however production cost of CC-LC system may be less than CC system.

References

- Filz, G. M. and Stewart, M. E. (2005). "Design of Bridging Layers in Geosynthetic-Reinforced, Column-Supported Embankments." *Virginia Transportation Research Council*, Charlottesville, VA.
- Vautrain J. (1980). "Comportement et dimensionnement des colonnes ballastées." *Revue Française de Géotech.* 11:59–73.
- Al-Khafaji ZA, Craig WH. (2000). "Drainage and reinforcement of soft clay tank foundation by sand columns." *Géotechnique* 50(6):709–13.
- Chen, Y.M., Jia, N., Chen, R.P., (2004). "Soil arch analysis of piled embankment." *China Journal of Highway and Transport.* 17 (4), 1–6 (in Chinese).
- Zhou DQ, Liu HL, Zhang KN. (2004). "Experimental comparison study on behavior of three and four-element composite foundation." *J Build Struct.* 25(5):124–9 [in Chinese].
- Chen Q. (2001). "Behavior of combined composite ground and simulation by study FEM." *Chin Civil Eng J.*, 34(1):50–5 [in Chinese].
- Yan ML, Wang MS, Yan XF, Zhang DG. (2003). "Study on the calculation method of multi-pile composite foundation." *Chin J Geotech Eng.*, 25(3):352–5 [in Chinese]. Zheng JJ, Abusharar SW, He C. (2005). "Design theory and application of CFG–lime piles composite ground." *In: 6th International conference on ground improvement techniques*, Coimbra, Portugal; p. 651–6.
- Varsuo, R.J., Grieshaber, J.B., Nataraj, M.S., (2005). "Geosynthetic reinforced levee test section on soft normally consolidated clays." *Geotextiles and Geomembranes* 23 (4), 362–384.
- Bergado, D.T., Teerawattanasuk, C., (2008). "2D and 3D numerical simulations of reinforced embankments on soft ground." *Geotextiles and Geomembranes* 26 (1), 39–55.

- Rowe, R.K., Skinner, G.D., (2001). "Numerical analysis of geosynthetic reinforced retaining wall constructed on a layered soil foundation." *Geotextiles and Geomembranes* 19 (7), 387–412.
- Skinner, G.D., Rowe, R.K., (2003). "Design and behaviour of geosynthetic reinforced soil walls constructed on yielding foundations." *Geosynthetics International* 10(6), 200–214.

Experimental Study on an Ideal Compaction Grouting into Sand

Shanyong Wang¹; Qiong Wang¹; Xinyu Ye¹; Scott William Sloan¹; and Daichao Sheng¹

¹ARC Centre of Excellence for Geotechnical Science and Engineering, Faculty of Engineering and Built Environment, Univ. of Newcastle, Australia. E-mail: shanyong.wang@newcastle.edu.au

Abstract: In this study, an ideal compaction grouting technique was designed by injecting grout into a special designed Latex balloon. In this way, the bleeding and penetration of grouts was avoided, and the extension of fractures could be limited. A large scale model test was accordingly developed to investigate the responses of the surrounding soils. After the application of an overburden pressure, pressure grouting was performed on sand samples, meanwhile, the evolution of grouting pressure, soil surface displacement, earth pressure as well as the void ratio at different distance from the injection point are monitored by various transducers. The results show that (i) the pressure grouting induced compaction effect in this study did not reach the up boundary of the model test; (ii) the earth pressure is obvious larger for the soil closer to the injection point; (iii) the densification effect decreases as the distance from the injection point increase, presenting clearly the density gradient around the injection point.

INTRODUCTION

A compaction grouting, also called displacement grouting, is a process where a high viscous grout is injected into the subgrade soil under pressure, during which the surrounded soil is displaced and at the same time compacted (Graf 1969, Warner and Brown 1974, Wang et al. 2013). However, in practice the radial and tangential stress redistribution, as well as excess pore water pressure generation, makes the actual mechanism of compaction grouting more complex, and careful control of the injection rate and pressure is needed to prevent fracture. On the other hand, due to the bleeding behavior in this process, it may not be feasible to exert pressure on the high viscous grout for extended time periods; the effect of compaction grouting is thus localized.

For this purpose, many researches have been conducted to investigate the mechanism of compaction grouting. For example, Younis (1994) performed laboratory compaction grouting tests to study grout bulb development and soil densification; Oakland and Bachand (2003) conducted a compaction grouting program to densify a zone of loose sand and silts. Kelesh and Matsui (2003) studied the effects of soil parameters, soil compressibility, replacement ratio and injection sequence on the effectiveness of compaction grouting through a field test. Soga et al. (2004)

investigated the compaction efficiency by measuring the deformation of clay specimens under axi-symmetrical conditions. Wang et al. (2010) investigated the behavior of compaction grouting under triaxial conditions, where the void ratio and excess pore water pressure were measured. However, all these studies considered just the global compaction behavior of the soil, the local response of soil around the grouting point is rarely investigated, although it reflects the real mechanism of the compaction grouting.

Therefore, in this study, an ideal compaction grouting technique is proposed by injecting grout into a special designed Latex balloon, during which the bleeding and penetration of grouts is avoided, and the extension of fractures could be limited. A large scale model test is accordingly developed to perform the test. By using a series of transducers, the responses of the surrounding soils in terms of surface displacement, the earth pressure as well as the void ratio changes were investigated. The results allowed the analysis of those parameter changes at different locations during grouting pressure increase, thus the earth pressure and densification effect gradients around the injection point were obtained.

EXPERIMENTAL METHODS

Materials tested

The soil tested is silica sand obtained from Stockton Beach, Newcastle, Australia. It consists 98.82% of quartz, 0.8% of rock fragments, 0.21% of Zircon, 0.11% of Ilmenite and 0.06% of Rutile (Ajalloeian et al. 1996). With a specific gravity of 2.67 Mg/m^3 , its maximum and minimum densities are 1.71 Mg/m^3 and 1.46 Mg/m^3 , respectively. It is classified as poorly graded sand by a uniformity coefficient C_u of 3.56 and a D_{50} close to 0.9 mm.

Experimental setup

The instruments used for the test are presented in Fig. 1. It consists of a model box and a pressure injection device. The model box is in 1000 mm long, 600 mm width and 730 mm height. This large volume of soil allows both the boundary effect being reduced and the monitoring of pressure and density changes gradient at different distance from the injection point. A drainage layer (10 mm thickness) made up of compacted gravel was used for the water/air release at bottom. While the top cover of the model box includes a Latex air bag, which was used to apply the overburden pressure. Two LVDTs were passed through the air bag and fixed with a PVC board to measure the soil surface displacement during both the overburden pressure application and pressure grouting process.

In order to perform the compaction grouting under an ideal condition, i.e. no bleeding and penetration condition, a special injection steel bar was designed. It was made of a hollow steel tube with inflatable balloon equipped (Fig.1). Two PVC tubes were passed through the hollow bar, one for the grout injection and another for the air release at the beginning of the injection process.

Around the balloon, five series of sensors were installed to monitor the soils response during the compaction grouting. Each series includes an earth pressure sensor and a volumetric water content sensor. Due to that there is no leakage of water from the inflatable balloon, the gravity water content of soil could be considered as

constant during compaction. Therefore, the volumetric water content variation at different location indicates actually the density changes induced by compaction grouting. The earth pressure sensor was employed to record the soil pressure and during compaction.

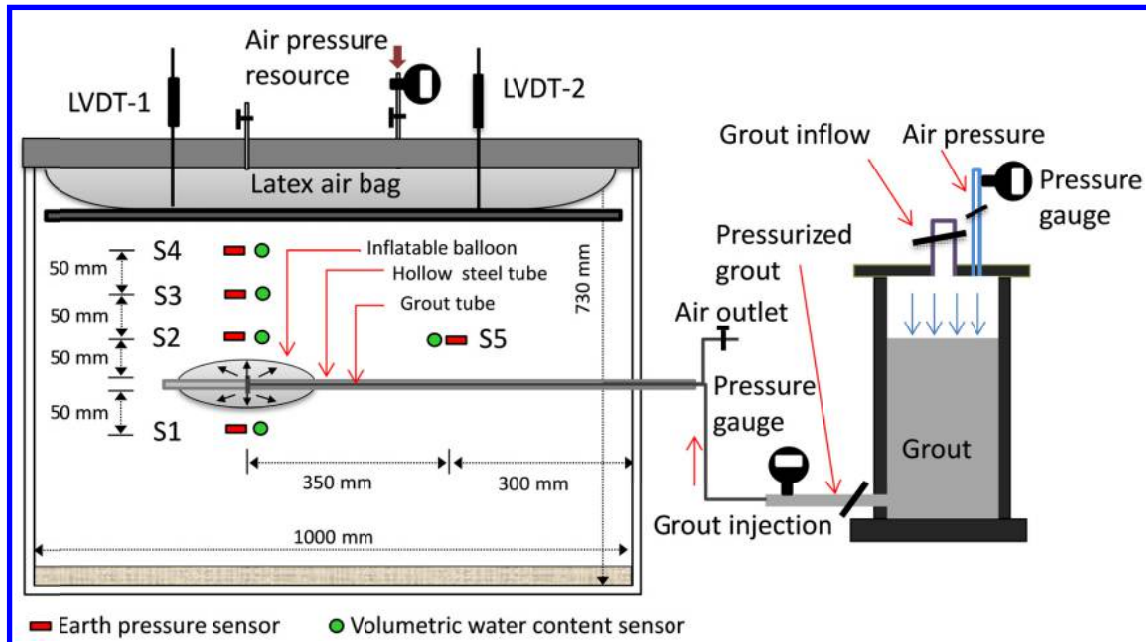


FIG. 1. Diagram of the experimental set up

The compaction grouting was realized by using the pressure grouting device shown in Fig.1. Air pressure was applied on the top to pressurize the grout into the inflatable balloon. Due to the fast set of the cement grout, it was impossible to exert the increasing grouting pressure step by step (100-200-300 kPa), the de-aired water was therefore injected. An air pressure regulator was used to adjust the increasing pressure, while two pressure gauges were used to measure the air pressure and injecting water pressure, respectively.

Experimental procedure

The compaction grouting was conducted on compacted sand samples at an initial void ratio of 0.8 and initial water content of 5%, corresponding to a degree of saturation of 20%. Compaction was performed layer by layer, the desired void ratio was reached by controlling the mass and volume of the soil. The grouting unit, i.e., steel bar with inflatable balloon, and measurement sensors were pre-placed during the compaction. The positions of those parts are presented in Fig.1.

As the compaction was completed, an overburden pressure of 100 kPa was firstly exerted on the top and kept almost constant thereafter (Fig. 2a). Once the sensors reading inside the soil sample reached the stability, the pressure grouting was started by applying three steps (100-200-300 kPa) of increasing pressure (see Fig. 2b). The earth pressure and volumetric water content were monitored, which allows the analysis of the soil responses due to the pressure grouting.

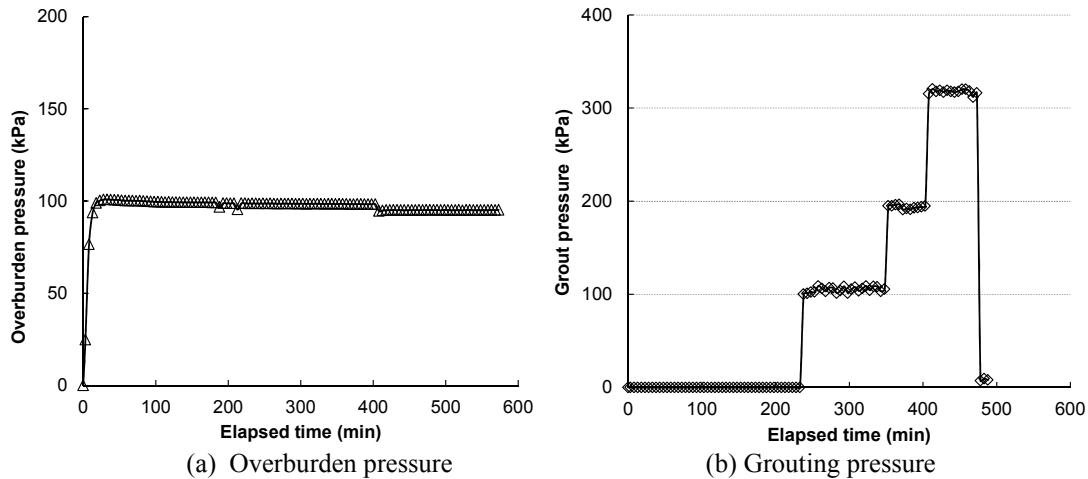


FIG. 2. Overburden pressure and grouting pressure applied

RESULTS AND DISCUSSION

Fig. 3. presents the soil surface displacement measured by the two LVDTs (see Fig. 1) during the test. It can be seen that as the 100 kPa of overburden pressure was applied, the soil surface settled rapidly and reached the stability after 1 hour. The final values are 32.76 mm and 31.34 mm at the two positions respectively (see Fig. 1 for the position), indicates an even surface settlement, and thus a good performance of the loading systems designed. However, no soil surface displacement was observed during the pressure grouting process. It implies that the pressure grouting induced compaction effect did not reach the soil surface (i.e., the up boundary of the model test) in this study.

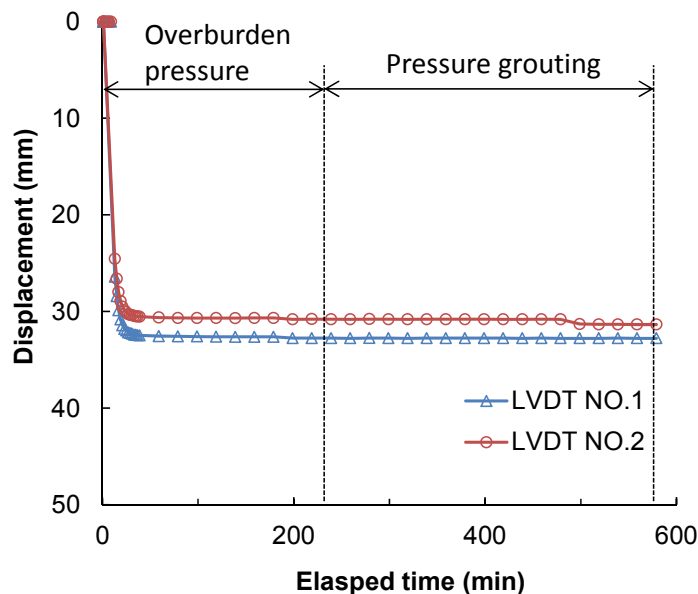


FIG. 3. Evolution of soil surface displacement

The changes of earth pressure at various positions are plotted in Fig.4. It can be seen that during the overburden pressure application, the stabilized earth pressure generally are in agreement with the overburden pressure of 100 kPa (Su et al. 2007). Upon pressure injection, no obvious changes of earth pressure were observed at grouting pressure of 100 kPa. When the grouting pressure increased to 200 kPa, earth pressures located around the injection point (i.e., S1-S4) increased slightly, then the subsequent increase of grouting pressure to 300 kPa caused the further increase of the earth pressure for S1 to S4. In addition, it can be observed that the closer from the injection point the larger the earth pressure is, expresses obviously the earth pressure gradient around the injection point. Meanwhile, the value for S5, which located at the same level of S2 but 350 mm far away from the injection point was kept unchanged.

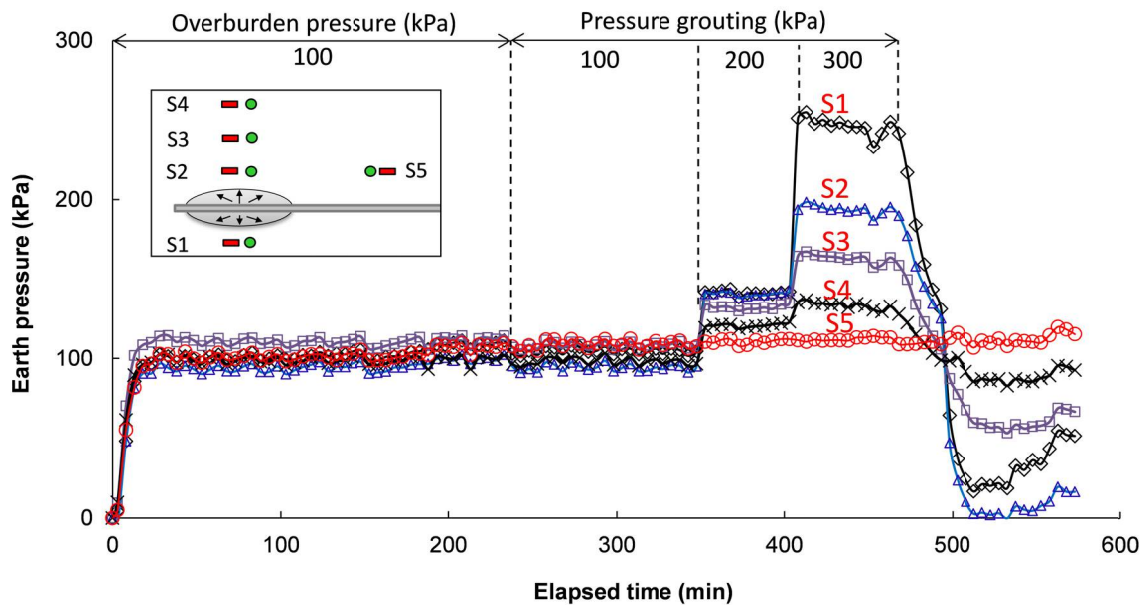


FIG. 4. Evolution of earth pressure

As mentioned above in this study, the volumetric water content sensors installed inside the soil sample were employed to monitor the densification effects around the injection point, giving that the gravity water content of the soil kept constant. Accordingly, the soil densities measured at each stage is plotted in Fig. 5. It was observed that the application of an overburden pressure induced significant decrease of void ratio. The final void ratios at different depth are well ordered according to the height of the sensors location (see S1-S4 in Fig. 5). It means that the influence of overburden pressure on the soil densification became less and less with depth, although the similar earth pressure at those locations (see Fig. 4). In addition, for the two sensors located at the same level (S2 and S5), the void ratio is 0.73 and 0.74, respectively, indicating similar densification effect. The slight differences between these two sensors are in agreement with the surface settlement in Fig. 3, which presents slightly larger settlement (32.76 mm) by LVDT-1 (on the top of the S2) compared to 31.34 mm for LVDT-2 (on the top of S5).